



# Volcanic tempo driven by rapid fluctuations in mantle temperature during large igneous province emplacement

Elliot J. Carter, Michael J. Stock, Adam Beresford-Browne, Mark R. Cooper, Robert Raine, Alexia Fereyrolles

## ► To cite this version:

Elliot J. Carter, Michael J. Stock, Adam Beresford-Browne, Mark R. Cooper, Robert Raine, et al.. Volcanic tempo driven by rapid fluctuations in mantle temperature during large igneous province emplacement. *Earth and Planetary Science Letters*, 2024, 644, 10.1016/j.epsl.2024.118903 . insu-04730595

**HAL Id: insu-04730595**

**<https://insu.hal.science/insu-04730595v1>**

Submitted on 10 Oct 2024

**HAL** is a multi-disciplinary open access archive for the deposit and dissemination of scientific research documents, whether they are published or not. The documents may come from teaching and research institutions in France or abroad, or from public or private research centers.

L'archive ouverte pluridisciplinaire **HAL**, est destinée au dépôt et à la diffusion de documents scientifiques de niveau recherche, publiés ou non, émanant des établissements d'enseignement et de recherche français ou étrangers, des laboratoires publics ou privés.



Distributed under a Creative Commons Attribution 4.0 International License



# Volcanic tempo driven by rapid fluctuations in mantle temperature during large igneous province emplacement

Elliot J. Carter<sup>a,b,\*</sup>, Michael J. Stock<sup>a</sup>, Adam Beresford-Browne<sup>c</sup>, Mark R. Cooper<sup>d</sup>, Robert Raine<sup>d</sup>, Alexia Fereyrolles<sup>e</sup>

<sup>a</sup> Department of Geology, Trinity College Dublin, College Green, Dublin 2, Ireland

<sup>b</sup> School of Geography, Geology and the Environment, Keele University, Staffordshire, ST5 5BG, UK

<sup>c</sup> School of Geography, Earth and Environmental Sciences, University of Birmingham, Birmingham, B15 2TT, UK

<sup>d</sup> Geological Survey of Northern Ireland, Dundonald House, Upper Newtownards Road, Belfast, BT4 3SB, UK

<sup>e</sup> Laboratoire Magmas et Volcans, Université Clermont Auvergne, 6 Avenue Blaise Pascal, 63170, Aubière, France

## ARTICLE INFO

Editor: Dr C. M. Petrone

### Keywords:

Large igneous province  
Basalt petrogenesis  
Geothermometry  
PRIMELT3  
Olivine-spinel thermometry  
Mantle plume  
Magmatic evolution  
North Atlantic

## ABSTRACT

The generation of Large Igneous Provinces (LIPs) is a topic of vigorous debate with competing models variably invoking hot mantle plumes, insulative heating by supercontinents or edge driven convective instabilities. Mantle temperature and its temporal variation during LIP magmatism is key to distinguishing between these different models. This may have important consequences for the dynamics, evolution and tempo of volcano-magmatic systems developed during these periods of intense activity. Despite this, there are currently no detailed stratigraphically constrained studies of mantle temperature through a LIP succession. To address this, we have applied both olivine-spinel thermometry and modelling of primary magma compositions (Monte Carlo PRIMELT3) to constrain mantle potential temperature through a continuous sequence of LIP lavas formed during the earliest expression of the North Atlantic Igneous Province (the Antrim Lava Group). Mantle potential temperature derived from olivine-spinel and olivine addition methods give consistent temperature ranges of 1403–1521 °C and 1374–1472 °C, respectively. However, both temperature records indicate significant (100–120 °C) variation in melting temperature over a relatively short stratigraphic interval during petrogenesis of early magmas and much less variation in later magmas, suggesting initial instability or pulsing which stabilised with time. This supports a plume origin for LIP formation. Variability in melting temperature is mirrored by proxies for crustal and volcanic processes; olivine Ni contents are elevated (<3000 ppm) in the same stratigraphic interval as the lowest mantle temperatures, indicating mixing of primary and more evolved (MgO ~4 %) melts, resulting from low magmatic flux into the crust during this time interval. The abundance and thickness of red weathering horizons capping lava flows is also significantly higher through the succession where mantle temperature variation is highest, indicating prolonged repose periods between eruption and a stop-start rhythm to volcanism. These unique observations indicate that volcanic, crustal and mantle systems are intrinsically linked and suggest that the tempo of volcanism, mediated via variations in melt flux, may ultimately be driven from below by changing mantle temperature.

## 1. Introduction

Large igneous provinces (LIPs) are the most volumetrically significant magmatic phenomena on Earth, extruding large volumes of lava over geologically rapid timescales and forming a key part of the global Wilson cycle (Black et al., 2021). Associated volatile emissions may play a significant role in altering Earth's climate and triggering mass extinction events (Clapham and Renne, 2019). The Plume Theory asserts

that LIP volcanism is caused by the heads of large (1000s km wide) plumes of hot material rising from near the core-mantle boundary (~2800 km) and impinging on the base of thinned lithosphere (e.g., Weis et al., 2023). This theory has gained broad, though not universal, acceptance for explaining key observations, including: very high melt production rates in LIP volcanism; apparent primordial <sup>3</sup>He/<sup>4</sup>He signatures in LIP magmas (Stuart et al., 2003); and volcanic trails between LIP and ocean island volcanism (Weis et al., 2023). Notable alternative

\* Corresponding author.

E-mail address: [e.carter2@keele.ac.uk](mailto:e.carter2@keele.ac.uk) (E.J. Carter).

<https://doi.org/10.1016/j.epsl.2024.118903>

Received 19 February 2024; Received in revised form 17 June 2024; Accepted 19 July 2024

Available online 22 August 2024

0012-821X/© 2024 The Author(s). Published by Elsevier B.V. This is an open access article under the CC BY license (<http://creativecommons.org/licenses/by/4.0/>).

theories posit that localised temperature excesses or melt production could arise either from long-term conductive insulation of the mantle by supercontinent lithosphere (Anderson et al., 1992), edge-driven convective instabilities (King, 2007), or more fusible heterogeneities in the mantle (Foulger and Anderson, 2005).

Prediction of excess heat and its temporal evolution is key to distinguish between competing theories for LIP and ocean island volcanism. In the simplest model, a plume head impacts the base of the lithosphere with a large heat anomaly over a wide area forming a LIP, and as the plume head transitions into a tail, temperature decreases and the area narrows forming ocean island or intraplate volcanism which potentially persists for millions of years (Campbell, 2007; Morgan, 1971). More complex episodic or oscillatory behaviour is predicted by some plume models (e.g., Olson et al., 1987). By contrast, “warm” insulated mantle models predict modest excess heat which dissipates rapidly during LIP magmatism (Meyer et al., 2007) and models invoking fusible mantle lithologies do not independently predict a temperature anomaly but are often combined with “warm” models to explain some of the unique geochemical aspects of LIP volcanism (e.g. Foulger and Anderson, 2005).

Secular variation in mantle temperature during LIP formation represents a significant change in the driving force for volcanism, and may impact the evolution and dynamics of magmatic and volcanic systems (e.g., Tapu et al., 2023). As a result, the exact mechanism of LIP formation may critically influence the volume and tempo of volcanic eruptions associated with their emplacement.

### 1.1. Determining mantle temperatures

Determining mantle potential temperature during LIP magmatism is crucial to distinguish between different geodynamic models. Mantle temperatures can be assessed via a range of geothermometers, based on chemical partitioning of different elements (Fe-Mg; Al; rare-earth elements, REE) between melt and minerals, as well as geophysical observations of crustal thickness. Olivine-melt thermometers rely on the temperature dependence of Fe-Mg partitioning between coexisting melt and residual mantle peridotite or crystallising olivine, respectively (Herzberg et al., 2007; Putirka, 2005). Olivine-spinel thermometry (“aluminium-in-olivine thermometry”) meanwhile, utilises the equilibrium partitioning of aluminium between olivine and spinel (Coogan et al., 2014). This method is generally regarded as more reliable than olivine-melt methods as it does not depend on assumptions regarding the composition of the melt with which the olivine is in equilibrium (Hole and Natland, 2020). Olivine-melt and olivine-spinel thermometers do not provide a melting temperature but rather a crystallisation temperature, which may be taken as a minimum melting temperature in sufficiently primitive melts. Melt-only methods employ reverse fractionation models to calculate a primary magma composition in equilibrium with peridotite and a temperature based on its MgO content (e.g., PRIMELT3; Herzberg and Asimow, 2015). These are complementary to olivine-based thermometers, however, their utility is limited by the requirement that magmas have only fractionated olivine in their liquid line of descent from primary melts. Clinopyroxene commonly crystallises in continental flood basalts and, without a reliable way to back-calculate the effects of multiphase fractionation, such methods yield erroneously high temperatures (Herzberg and Asimow, 2015).

Mineral and melt thermometry has been used to show temperature anomalies during LIP volcanism as well as apparent secular cooling between LIP emplacement and associated later intraplate volcanism (Coogan et al., 2014; Herzberg and Gazel, 2009; Trela et al., 2017). However, many studies, particularly those of the North Atlantic Igneous Province, have suggested more complex behaviour, including temperature increases (Spice et al., 2016), or even oscillatory behaviour (Parnell-Turner et al., 2014). Furthermore, many LIPs record significant ranges in temperature, even within a restricted range of time and space (Hole and Millett, 2016). Collectively, such observations pose a

challenge to theories of insulative mantle warming, which lack a clear mechanism by which temperature may resurge following latent heat release by LIP volcanism.

Discriminating between models of LIP formation requires a detailed understanding of the temporal evolution of mantle temperatures; the rapidity of temperature changes directly relates to modes of formation. However, while several studies have demonstrated broad secular variation in mantle temperatures between tectonically established groups with 1–20 Myr age differences (e.g., Herzberg and Gazel, 2009; Spice et al., 2016; Thompson and Gibson, 2000), such variation in mantle temperature is yet to be quantified within a detailed (<1 Myr) stratigraphic framework. Several sources have considered influence of steady state or waning plumes on crustal architecture (e.g. Black et al., 2021; Tapu et al., 2023) but none have looked at the potential influence of oscillating temperature on crustal systems, nor coupled studies of crustal magmatic systems to independently determined mantle temperatures. As a result, it has not been possible to assess how mantle temperature variations influence the dynamics of associated crustal magmatic and volcanics systems.

Here we apply, for the first time, both PRIMELT3 modelling and olivine-spinel geothermometry to a well-constrained stratigraphy of primitive LIP basalts from the North Atlantic Igneous Province. In the case of PRIMELT3 temperatures, we apply a novel Monte Carlo-based approach (MC-PRIMELT3) to account for ubiquitous augite fractionation and recover temperatures generally in good agreement with those from olivine-spinel thermometry. Together, these data allow us to examine a temporal record of LIP melting in unprecedented detail and demonstrate rapid variation of up to 120 °C in mantle potential temperatures during the early onset of a major LIP. We integrate this with proxies for magmatic flux and the frequency of volcanic eruptions, ultimately demonstrating a fundamental link between mantle, crustal and volcanic systems during LIP emplacement.

## 2. Geological setting

### 2.1. The North Atlantic Igneous Province

The North Atlantic Igneous Province (NAIP) is one of the best studied LIPs on Earth, with exposures widely distributed on both sides of the Atlantic. It initiated at ~62 Ma and was emplaced in two main phases (Saunders et al., 1997): Phase 1 preceded rifting and includes successions in West Greenland, Baffin Island, and the British and Irish portion of the province (collectively termed the British and Irish Paleogene Igneous Province; BIPIP). Initial volcanism was widespread and roughly synchronous over an area ~2000 km in diameter. Phase 2 formed during rifting and encompasses much of the East Greenland sequence, the Greenland-Iceland-Faroes aseismic ridge, and thick sequences of seaward dipping reflectors along the NW European and E Greenland continental margins.

A number of studies have contrasted Phase 1 NAIP magmas with those of modern Iceland (Chambers and Fitton, 2000; Fitton et al., 1997; Hole, 2018). The latter are characterised by isotopic and trace element heterogeneity which is associated with major element variation and ascribed to a proportion (~4–15 %) of hybrid-pyroxenite or eclogite in their mantle source (Shorttle et al., 2014; Shorttle and MacLennan, 2011), whereas there is limited evidence for a significant pyroxenite contribution to Phase 1 NAIP magmas, especially in the BIPIP (Hole, 2018). Rather, on the basis of distinction in high field strength element composition, studies have argued for a temporal transition in mantle source late in the emplacement of the BIPIP from a mid-ocean ridge basalt (MORB)-like source to one more typical of modern day Iceland (Chambers and Fitton, 2000; Fitton et al., 1997; Kent and Fitton, 2000).

### 2.2. The Antrim Lava Group

Extrusive portions of the BIPIP are located in the Scottish Hebrides

(Mull, Skye, Rhum, Small Isles, Eigg, Muck) and Northern Ireland, which preserves the largest onshore exposure, forming the Antrim Plateau (Fig. 1). Successions exposed in the Hebrides principally consist of alkali or transitional alkali-tholeiitic olivine basalts with rare (<10 vol.%) more-evolved flows (Bailey et al., 1924; Saunders et al., 1997). The thickest successions on Skye and Mull are ~1200 m and ~1800 m thick, respectively, and are capped by tholeiites.

The Antrim Lava Group (ALG) encompasses the Northern Irish lavas of the NAIP, covering an area of 3500 km<sup>2</sup> and up to 800 m thick. It principally consists of two main lava sequences, the older Lower Basalt Formation (LBF) and the younger Upper Basalt Formation (UBF; Fig. 1; Cooper, 2004). The interval between these two is punctuated by eruption of the Tardree Rhyolite Complex (TRC) - a series of silicic domes, flows and pyroclastic units - and the Causeway Tholeiite Formation (CTF), the latter of which forms the columnar jointed flows of the Giant's Causeway (Lyle and Preston, 1993; Patterson and Swaine, 1955). Apart from these relatively localised extrusions, the interval between Upper and Lower Basalts is characterised by a marked hiatus in volcanism during which thick laterites formed (>30 m thick in places; Hill et al., 2000).

Compared to Hebridean Palaeogene volcanics, the Antrim lavas have been comparatively under studied. Nonetheless, geochemical investigations in the 1980s and 1990s included major and trace elements (Lyle, 1985; Lyle and Patton, 1989) as well as Sr, Nd and Pb isotopes (Barrat and Nesbitt, 1996; Ellam and Stuart, 2000; Wallace et al., 1994). Lower and Upper Basalt REE profiles show heavy REE depletion and record deep melting, partially within the garnet stability field, similar to many BIIP magmas (Barrat and Nesbitt, 1996). The Causeway Tholeiite is an exception with a flatter pattern indicative of shallower melting entirely in the presence of spinel, and with LREE enrichment attesting to substantial assimilation of continental crust. Sr and Nd isotopes in the two main basalt sequences indicate variable interaction with crustal

lithologies, with isotopic ratios ranging from nearly uncontaminated mantle values to somewhat elevated values ( $^{87}\text{Sr}/^{86}\text{Sr}$  0.7029–0.7084; Wallace et al., 1994). The CTF shows a higher degree of crustal influence ( $^{87}\text{Sr}/^{86}\text{Sr}$  = 0.704–0.716) (Barrat and Nesbitt, 1996; Wallace et al., 1994). Lower and Upper Basalts have no correlation between Sr isotopes and major elements for mafic samples (MgO > 5 %), indicating that crustal assimilation has not detectably perturbed the major element composition of the primary magmas. The tholeiites, by contrast, show strong correlations between  $^{87}\text{Sr}/^{86}\text{Sr}$  and a range of major and trace elements (Barrat and Nesbitt, 1996; Wallace et al., 1994).

### 2.3. Temperatures in the NAIP

Reliable estimates of melting temperature for the NAIP come principally from olivine-spinel thermometry (Coogan et al., 2014; Spice et al., 2016) and olivine-addition methods to determine a primary melt composition (e.g. PRIMELT3; Hole and Millett, 2016; Hole and Natland, 2020), although some insight has been gained from REE inversions (MacLennan et al., 2001) and considerations of crustal thickness in Iceland (e.g., Parnell-Turner et al., 2014). Almost all studies agree that there is a thermal anomaly associated with NAIP magmatism, although some do not directly calculate a mantle potential temperature ( $T_p$ ) but rather compare crystallisation temperatures in MORB and LIPs and assume any difference corresponds to a difference in  $T_p$  (e.g., Coogan et al., 2014; Spice et al., 2016). Several studies show or infer large temperature excesses of up to 300 °C in the NAIP. Taking ambient mantle  $T_p$  as 1350 °C (Herzberg et al., 2007), this suggests  $T_p$  <1650 °C (Herzberg and Gazel, 2009; Hole and Millett, 2016; Spice et al., 2016), whereas other datasets suggest more modest maximum  $T_p$  of 1500–1550 °C (Coogan et al., 2014; Hole and Natland, 2020). Hole and Millett (2016) showed apparent temperature zonation in the early NAIP with the highest temperatures (>1600 °C) in West Greenland and somewhat lower

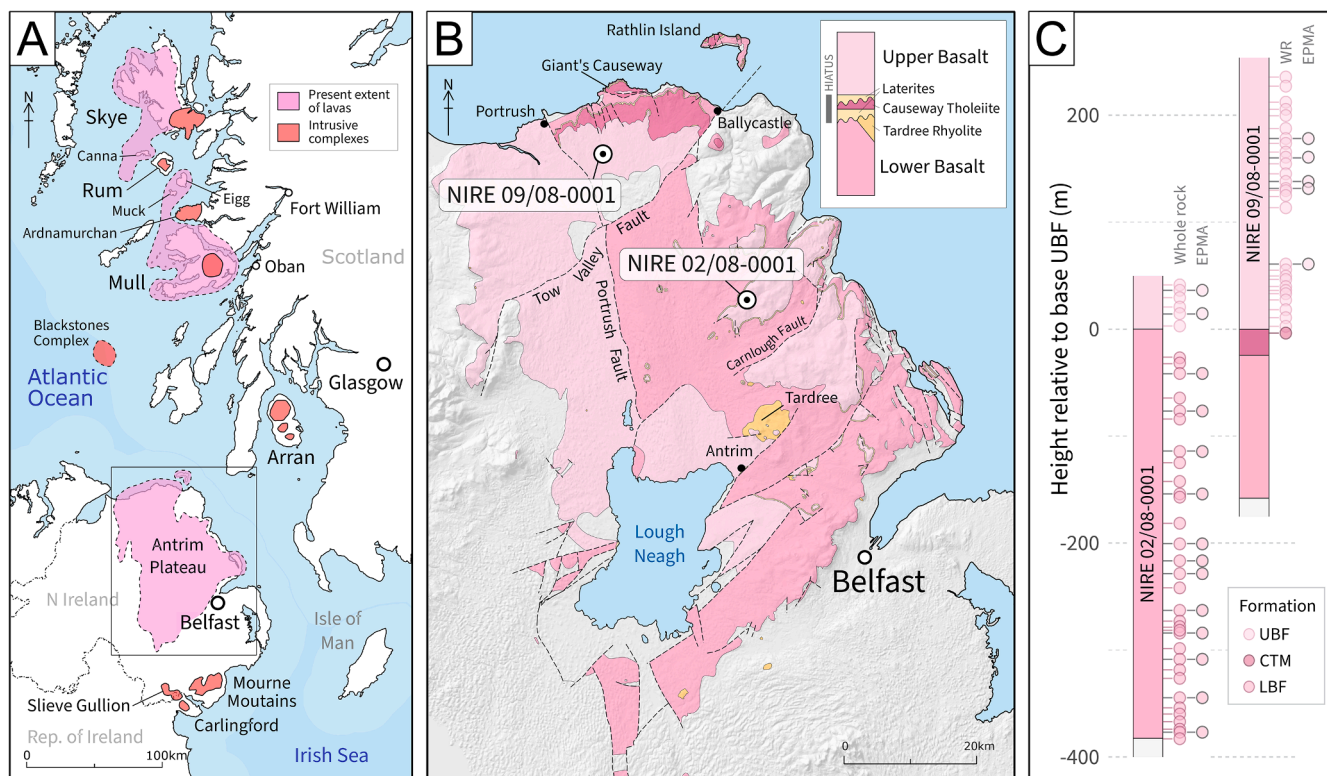


**Fig. 1.** Geological setting, location and samples. A – schematic geological map showing locations and extent of extrusive and intrusive portions of the British and Irish Paleogene Igneous Province (adapted from Cooper, 2004). B – geological map of the Antrim Plateau showing the location of sampled boreholes and other key localities with stratigraphy summarised in inset (contains data from 1:250k Geological Map of Northern Ireland, GSNI); fault locations taken from Anderson et al., 2016). C – stratigraphy of boreholes showing depths of samples for whole rock analysis and electron-probe microanalysis (EPMA).



temperatures ( $<1563^{\circ}\text{C}$ ) in BIPIP magmas, taken to have formed on the margins of the plume.

Temperature estimates for modern Iceland are elevated from ambient mantle but less than earlier phases of the NAIP, with  $T_p$  ranging  $1396\text{--}1527^{\circ}\text{C}$ . This has been interpreted as secular cooling in the Icelandic plume (Herzberg and Gazel, 2009; Spice et al., 2016). Matthews et al. (2021, 2016) provide a detailed examination of the assumptions underlying olivine-spinel  $T_p$  determinations and, with additional constraints from crustal thickness and melting lithology, estimate a narrower range of  $T_p$  from  $1507$  to  $1546^{\circ}\text{C}$  for modern Iceland.

A common feature of existing data is a large range of temperature estimates at a given time and location. Temperature ranges exceeding  $100^{\circ}\text{C}$ , well outside of analytical uncertainty, exist within the BIPIP despite its comparatively restricted area (Hole and Millett, 2016; Spice et al., 2016), with Hole and Millett (2016) explicitly commenting that the assumption of steady state temperature appeared to be invalid for the NAIP. Despite this, the exact nature and tempo of this temperature variation remains unclear due to the lack of stratigraphic detail in previous studies.

### 3. Samples and methodology

The ALG has been cored for mineral exploration at multiple sites by LonMin PLC, with cores archived at the Geological Survey of Northern Ireland. These allow detailed sampling and logging of a continuous stratigraphically-controlled succession through the entire thickness of the ALG. A composite section was constructed from the two most complete sequences (NIRE 02/08–0001, NIRE 09/08–0001; Fig. 1) which can be correlated at the extensively lateritised interval between the Upper and Lower Basalt Formations (Fig. 1).

Each of the 67 flows in the composite section was sampled, cleaned and studied in hand specimen under a binocular microscope to identify any phenocrysts and qualitatively assess their abundance before being powdered for bulk rock analysis. A subset of 30 samples spaced throughout the composite section were prepared as thin sections and studied under transmitted polarising light and by scanning electron microscopy. The samples range from aphyric to olivine-phyric basalts with phenocryst assemblages consisting of olivine ( $1\text{--}23\text{ vol}\%$ )  $\pm$  plagioclase ( $0\text{--}7\text{ vol}\%$ ) with no phenocrystic clinopyroxene (Fig. S1). Some samples contain intergrown olivine and plagioclase phenocrysts with rounded grain boundaries (Fig. S2), which likely derive from a disaggregated mush (Holness et al. 2019). The groundmass is microcrystalline, containing plagioclase ( $\pm$  olivine) enclosed by oikocrystic augite.

The major and trace element compositions of powdered samples were determined by wavelength dispersive X-Ray Fluorescence Spectroscopy (XRF) on fused glass beads and pressed powder pellets, respectively (Supplementary Table S1). Analyses were collected using the Zetium instrument in the Earth Surface Research Laboratory, Trinity College Dublin. For major elements, relative accuracy was typically  $<3\%$  and precision  $<0.5\%$ . For trace elements, relative accuracy was typically  $1\text{--}10\%$  and precision  $0.5\text{--}5\%$  with both parameters correlating inversely with concentration (Supplementary Table S2). Full analytical details for this and other analyses are given in Supplementary Text S3.

Olivine, spinel and plagioclase compositions were determined using a Cameca SX100 electron microprobe (EPMA) in the Department of Earth Sciences, University of Cambridge. For each olivine-spinel pair, three or more olivine analyses were made arranged in a triangle around the spinel. The mean of the olivine analyses was then taken to approximate the composition at the spinel-olivine contact. Full EPMA analytical conditions are in Supplementary Table S4.

#### 3.2. Calculating mantle $T_p$ from olivine-spinel thermometry

Olivine-spinel crystallisation temperatures were calculated using the

Al-exchange thermometer of Coogan et al. (2014). This provides a crystallisation temperature for the olivine-spinel pair. Where these are primitive (olivine forsterite,  $\text{Fo} > 80\text{ mol}\%$ ), as in the majority of analysed ALG olivines, this provides a minimum temperature of melting (since the temperature of crystallisation must be less than that of melting). However, ALG olivines are somewhat less forsteritic than compositions expected to be in equilibrium with primary mantle melts ( $\sim\text{Fo}91$ ) indicating some fractional crystallisation has occurred. As a result, we apply a back calculation to reach a primary crystallisation temperature (e.g., Matthews et al., 2021) as well as corrections for latent heat and adiabatic heat loss to calculate a potential temperature (Putirka, 2005; Supplementary Text S4.2). Calculation of  $T_p$  from  $T_{\text{cryst}}$  was performed assuming a homogeneous lherzolitic mantle source (see Supplementary Text S4.2.3 for full justification).

To account for uncertainties in the slope of the melt + ol  $\pm$  cpx liquid line of descent (LLD), the pressure of melting, and fraction of melting, a Monte Carlo model was implemented, with each of these parameters randomly sampled 2500 times within a normal distribution. The slope of the LLD was taken from averaging multiple Petrolog3 model LLDs run over a range of pressure ( $1\text{--}2\text{ GPa}$ ) and starting compositions (Table S7). The pressure distribution of melt segregation was calculated from the composition of primary melts calculated by Monte Carlo olivine + clinopyroxene addition (see Section 3.3.), using the barometer of Lee et al. (2009; Table S8). The respective means and standard deviations used were  $\delta T/\delta \text{Fo} = 12.2 \pm 1.5^{\circ}\text{C/mol}\%$ ,  $P_{\text{melt}} = 1.72 \pm 0.25\text{ GPa}$ , and  $F = 0.22 \pm 0.043$ . The adiabatic gradient was taken as  $18\text{ K/GPa}$  (Katsura, 2022) and all other parameters follow Putirka (2005). Our approach, assumptions underlying this calculation and the derivation of these parameters are detailed in Supplementary Text S4.2.

#### 3.3. Determining temperature using PRIMELT3 in clinopyroxene-saturated magmas

Melting temperatures can also be determined from the composition of a melt using models such as PRIMELT3 (Herzberg and Asimow, 2015) which applies an olivine inverse fractionation model to a measured lava compositions, calculating a primary magma composition and associated melting temperature. However, such methods make the assumption of olivine-only fractionation, which may be invalid for any ALG samples which have undergone clinopyroxene crystallisation, potentially resulting in systematic overestimation of  $T_{\text{melt}}$  (Herzberg and Asimow, 2015). Various approaches have been applied to the problem of additional crystallising components including: graphical analysis (e.g. Till et al., 2012); thermodynamic models (Danyushevsky and Plechov, 2011); and search methods which find a candidate primary magma from which a given co-/eutectic melt could evolve (e.g. Kimura and Ariskin, 2014). However, a common problem is that small uncertainties in the initial conditions of the inversion compound to large, poorly constrained uncertainties in the solution (Herzberg and Asimow, 2015).

Most ALG samples have low CaO for a given Mg# (Fig. 2) resulting from fractional crystallisation of clinopyroxene. There is no evidence that low CaO contents are due to melting of pyroxenite (Supplementary Text S4.1.2). To address the issue of clinopyroxene saturation in our samples, we have developed a novel Monte Carlo-based approach whereby a large population of candidate primary melts are created by projecting from points along the olivine-only reverse fractionation path towards a database of experimental clinopyroxene compositions (LEPR, Hirschmann et al., 2008;  $n = 106$ ,  $P = 1.2\text{--}2.0\text{ GPa}$ ,  $T = 1250\text{--}1500^{\circ}\text{C}$ ). Where projections intersect the FeO/MgO of primary mantle melts ( $0.56 \pm 0.02$ ; Hole and Millett, 2016), a candidate primary melt for the sample is generated. These candidate melts are then filtered to those with CaO concentrations consistent with primary peridotite melts (Herzberg and Asimow, 2008) before being reininput to PRIMELT3 to check for internal self-consistency and calculate a temperature (Herzberg and Asimow, 2015; Table S8). This method is referred to as Monte Carlo PRIMELT3 (MC-PRIMELT3) hereafter.

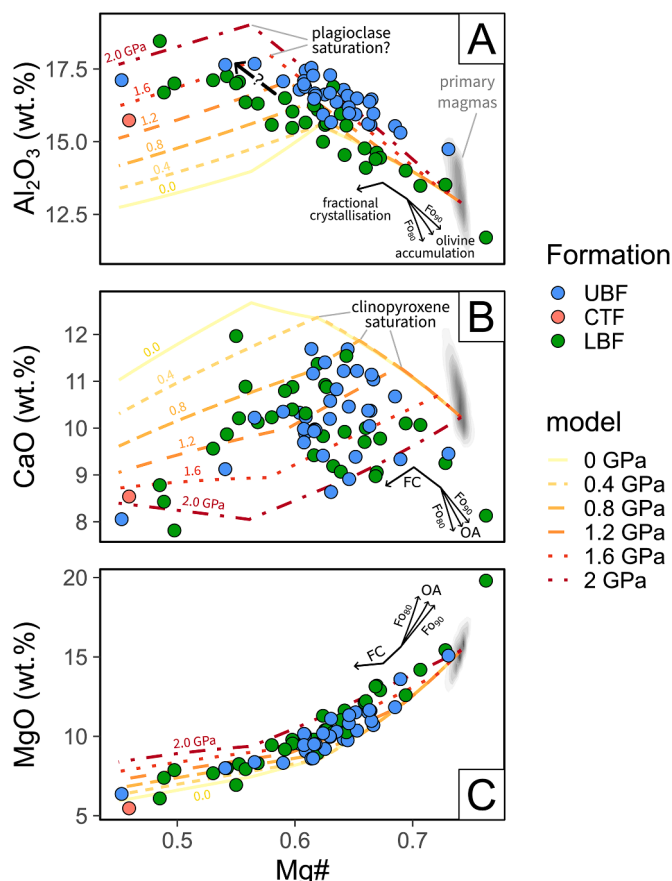


**Fig. 2.** Harker plots showing magmatic differentiation for all ALG samples. A –  $\text{Al}_2\text{O}_3$  versus  $\text{Mg\#}$  (molar  $\text{Mg}/[\text{Mg} + \text{Fe}]$ ) showing negative correlation for almost all samples. Only samples with  $\text{Mg\#} < 0.5$  appear to have fractionated plagioclase. B –  $\text{CaO}$  versus  $\text{Mg\#}$  showing low  $\text{CaO}$  for a given  $\text{Mg\#}$  indicating clinopyroxene fractionation has taken place. C –  $\text{MgO}$  versus  $\text{Mg\#}$ . The compositions of primary magmas calculated by MC-PRIMELT3 is shown as a grey cloud (Supplementary Table S8). LLDs calculated in Petrolog3 (Danyushevsky and Plechov, 2011) for a range of pressures (0–2 GPa) are shown (see Supplementary Text S4 for details). Vectors for fractional crystallisation and addition of olivine (Fo 80–90 mol%) are shown in each panel.

To avoid issues associated with xenocrystic olivine accumulation, the composition of olivine-phyric samples was recalculated as olivine-free using olivine abundances determined by image analysis (Supplementary Text S3.3) and the composition of olivine measured by EPMA (Table S3). All whole-rock or liquid compositions used for calculating temperatures had  $\text{MgO} > 10$  wt% and, to avoid extra complexity associated with potential plagioclase fractionation, a small number of samples either with plagioclase macrocrysts or with  $\text{MgO}/\text{Al}_2\text{O}_3 < 0.55$  were discarded, following Hole and Natland (2020). The modelling approach is illustrated for two samples in Fig. 3 and full details are given in Supplementary Text S4.3.

This approach implicitly includes the uncertainty of the exact crystallisation paths and therefore has a large advantage over a deterministic back fractionation model which would give an apparently unique answer without quantifying the large uncertainties linked to the LLD, pressure-temperature conditions, and final composition. The output of our model is a range of primary mantle melts that are possible via olivine + clinopyroxene fractionation for a given starting composition, each with an associated  $T_p$ , approximating a normal distribution.

#### 4. Results

All samples have whole-rock major element chemistry consistent

with primitive olivine-normative basalts.  $\text{SiO}_2$  ranges from 45 to 48 wt %, whereas  $\text{MgO}$  and  $\text{Mg\#}$  (molar  $\text{Mg}/[\text{Mg} + \text{Fe}]$ ) are more variable, ranging 6–19 wt% and 45–76 mol%, respectively (Fig. 2). Sample AB-B929 from the CTF is distinct with higher  $\text{SiO}_2$  (51.3 %) and slightly lower  $\text{MgO}$  (5.5 %). Most elements show incompatible behaviour in high  $\text{Mg\#}$  whole-rock analyses, consistent with olivine-only crystallisation (Fig. 2; Fig. S5).  $\text{CaO}$  shows an inflection at  $\text{Mg\#} \sim 60$ , switching to compatible behaviour where clinopyroxene comes onto the liquidus.  $\text{Al}_2\text{O}_3$  and  $\text{Na}_2\text{O}$  correlate negatively with  $\text{Mg\#}$  in all samples, suggesting plagioclase did not saturate in most magmas, consistent with the near absence of plagioclase phenocrysts in our samples.

The forsterite (Fo;  $\text{Mg}_2\text{SiO}_4$ ) contents of olivine phenocryst cores range 69.0–88.7 mol% (mean  $83.9 \pm 2.8$ ,  $1\sigma$ ;  $n = 590$ ), while mantles range 67.4–86.3 (mean  $80.1 \pm 3.8$ ,  $n = 135$ ), and rims range 81.6–56.5 mol% (mean  $69.4 \pm 7.5$ ,  $n = 52$ ). Olivine  $\text{P}_2\text{O}_5$  contents are low ( $< 0.07$  wt%) and  $\text{CaO}$  shows a narrow range (0.2–0.4 wt%), typical of magmatic olivine (Thompson and Gibson, 2000).

Spinel  $\text{Mg\#}$  spans 21.1–68.9 mol% and  $\text{Cr\#}$  (molar  $\text{Cr}/[\text{Cr} + \text{Al}]$ ) ranges from 10.2 to 53.5 mol%.  $\text{TiO}_2$  is generally within the calibration range of the Coogan et al. (2014) olivine-spinel thermometer, typically ranging 0.1–1.1 wt% (mean  $0.5 \pm 0.2$ ,  $n = 346$ ). A small number ( $n = 28$ ) of spinels with elevated  $\text{Fe}^{3+}$  and/or  $\text{TiO}_2$  contents outside of the thermometer calibration were excluded from temperature calculations (Supplementary Text S4.2).

After filtering for spinel  $\text{TiO}_2$  and  $\text{Fe}^{3+}$  contents, 240 olivine-spinel pairs from 18 samples yielded calculable temperatures, with 1–30 temperatures per sample (Table S5). Uncorrected crystallisation temperatures range 1176–1363 °C, with the full range of temperatures recorded in the dataset present in data from the most primitive olivines ( $\text{Fo} > 84$  mol%;  $n = 126$ ). Once corrected for crystallisation, latent heat and adiabatic heat loss (Supplementary Text S4.2),  $T_p$  for individual olivine spinel pairs ranges 1403–1521 °C with both maximum and minimum temperatures recorded in the LBF. The UBF shows a significantly narrower range of  $T_p$  from 1425 to 1469 °C (Fig. 4; Supplementary Table S9).

Two samples (ABB002 and ABB908), both aphyric or very poorly phyric and from the UBF, yielded temperatures directly via PRIMELT3 solutions (without warnings for augite fractionation). These resulted in calculated mantle  $T_p$  of 1457 and 1466 °C, respectively. All other samples had  $\text{CaO}$  contents too low to be related to primary peridotite melts by olivine-only fractionation. After applying our Monte Carlo approach to reverse clinopyroxene crystallisation (MC-PRIMELT3; Supplementary Text S4.3), these samples yielded PRIMELT3 solutions with mean  $T_p$  for each sample ranging 1374–1472 °C (Supplementary Table S10).

#### 5. Discussion

##### 5.1. A stratigraphic record of mantle temperature

Our MC-PRIMELT3 and corrected olivine-spinel thermometry outputs provide two comparable temporal records of mantle potential temperature ( $T_p$ ) and, for both datasets, we consider the mean as the best estimate of  $T_p$  for each individual sample (See Supplementary Text S4.2.2). Mean  $T_p$  values show marked variation in our sample set, ranging 1403–1521 °C ( $\Delta T = 117$  °C) for olivine-spinel temperatures and 1374–1472 °C ( $\Delta T = 98$  °C) for MC-PRIMELT3 temperatures (Fig. 4). Both the absolute  $T_p$  values for each sample and the magnitude of relative variations along our composite log show a good agreement between the two independent temperature records albeit with a slight vertical offset between the two records (see Section 5.1.1 below). Our calculated temperatures are consistent with most previous estimates of mantle  $T_p$  in the NAIP in indicating modest excess mantle temperatures (+100–150 °C). They also extend to markedly low temperatures, little above ambient mantle ( $T_p \sim 1350$  °C; Herzberg et al., 2007).

There is a marked difference in the degree of  $T_p$  variability between the Upper and Lower basalts. For both olivine-spinel and MC-PRIMELT3

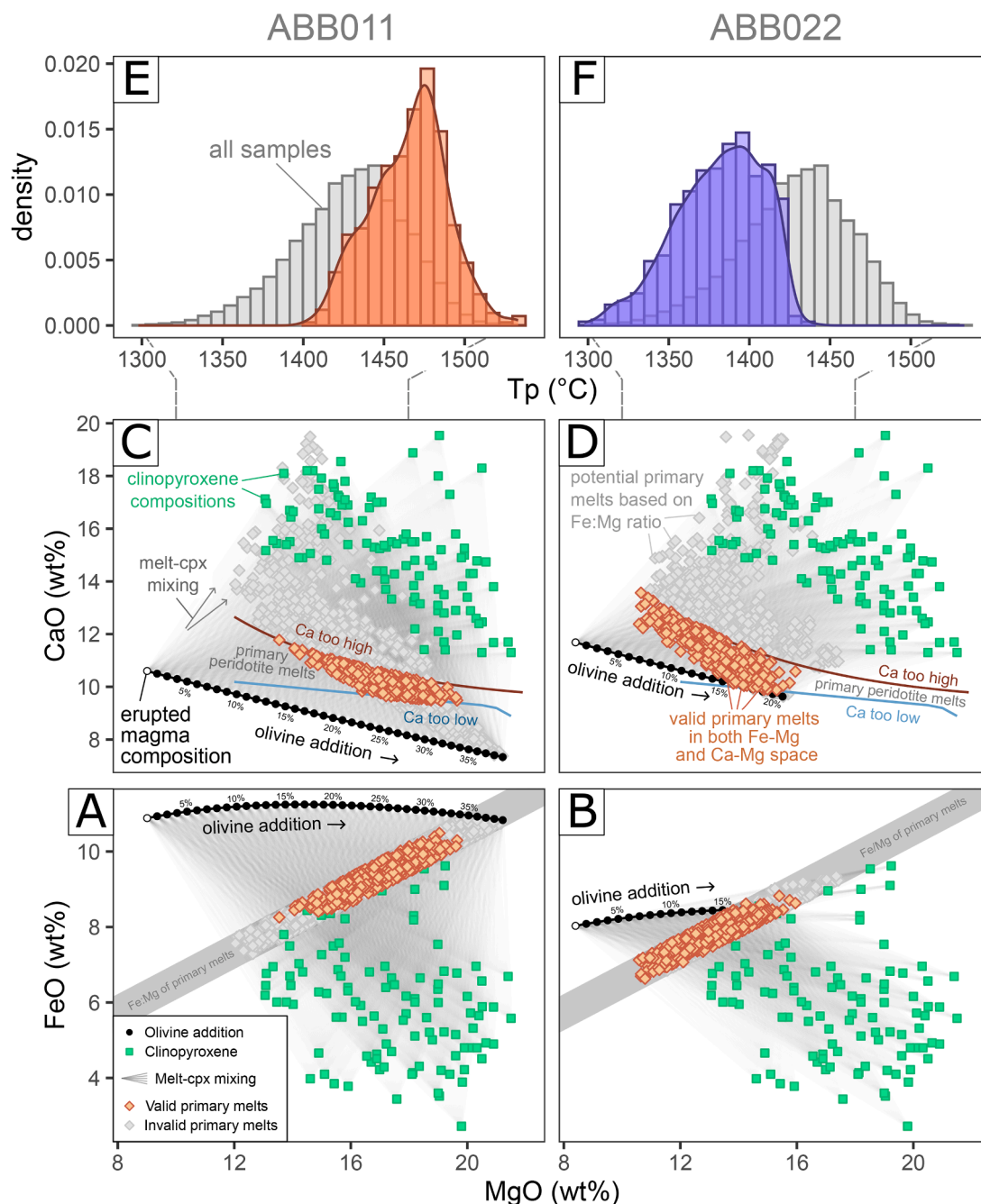


**Fig. 3.** Monte Carlo approach for reversing olivine and clinopyroxene crystallisation to calculate primary magma compositions and an associated potential temperature (MC-PRIMELT3). Two samples (ABB011 and ABB022) are shown as examples; for corresponding plots for every sample, see Supplementary Figure S12. A & B – FeO versus MgO showing projections (grey lines) from all points along an olivine addition reverse fractionation path (black points; erupted liquid composition in white) to multiple experimental clinopyroxene compositions (green squares). Where the projection intersects the zone of primary melts (grey diagonal bar) a candidate primary melt is generated (grey and orange diamonds). C & D – CaO versus MgO for the same LLDs, clinopyroxenes and projected melt compositions. Candidate primary melts are filtered into valid (orange diamonds) and invalid (grey diamonds) primary melts based on whether their CaO contents are consistent with melting of peridotite (bounds shown by red and blue curves; [Herzberg and Asimow, 2015](#)). E & F – histogram of mantle potential temperatures for all valid primary melts in A - D. A histogram of temperatures for all samples is shown in grey for comparison.

temperatures, LBF samples shows a wider range of temperatures than UBF and encompass both maximum and minimum temperatures. While the LBF records the full range of temperature in the dataset ( $\Delta T_{\text{olivine-spinel}} = 117^\circ\text{C}$ ,  $\Delta T_{\text{primelt}} = 98^\circ\text{C}$ ), temperature variation among UBF samples is  $\sim 30\text{--}50\%$  of that in the LBF ( $\Delta T_{\text{olivine-spinel}} = 45^\circ\text{C}$ ,  $\Delta T_{\text{primelt}} = 53^\circ\text{C}$ ). A variety of statistical tests including ANOVA, post-hoc Tukey and F tests indicate that these differences are statistically significant to  $p < 0.05$  (Supplementary Text S5). Both records therefore indicate that  $T_p$  varied significantly during melting to form the earliest ALG magmas and

became more stable with time.

Variation in mantle  $T_p$  will cause variation in the degrees of melting, significantly affecting the major and trace element contents of melts. Lower temperatures are expected to correspond to lower degrees of melting and higher incompatible element concentrations in the resulting melts. However, isotopic data suggest that most BIPI basalts are contaminated by interaction with small volumes of continental crust which, with the exception of Nb/Zr ratios, appears to have perturbed their trace element systematics but not significantly disturbed the major

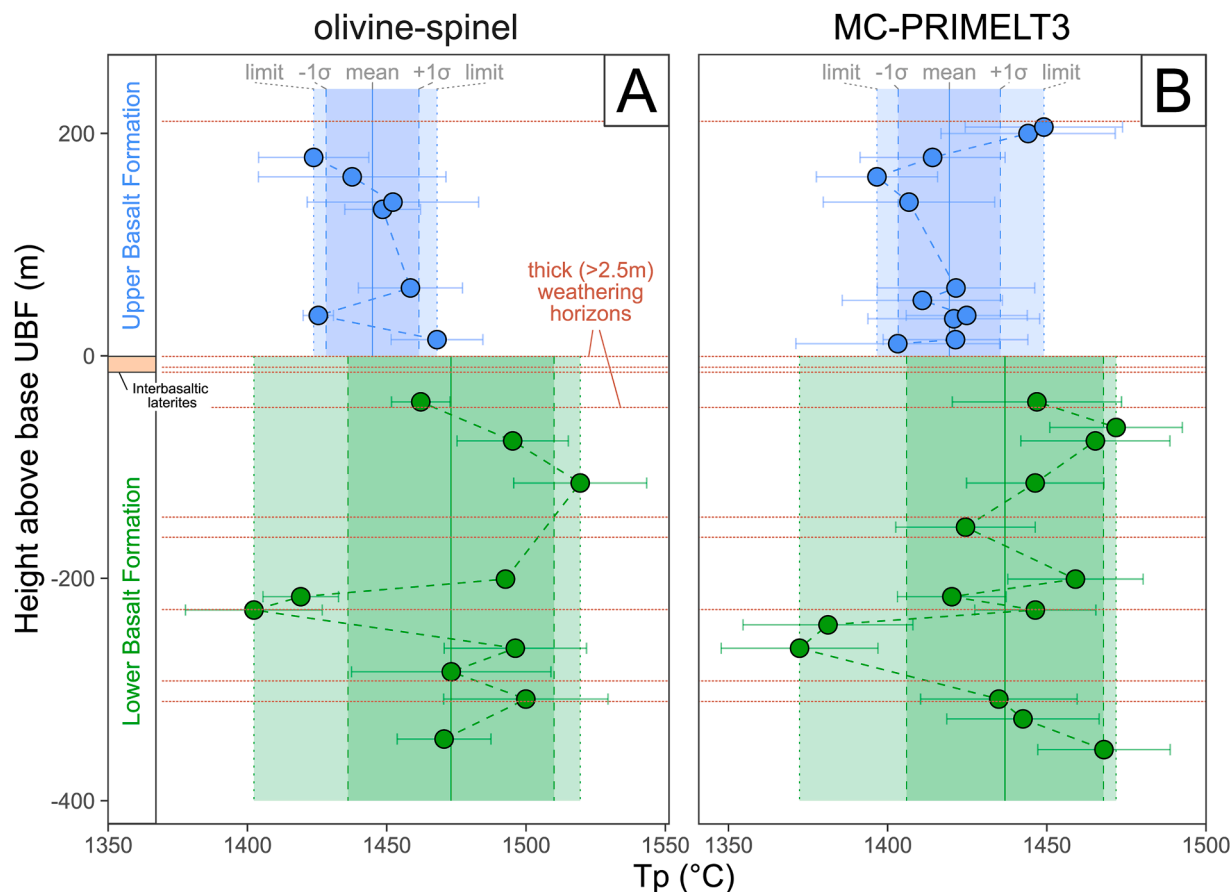


**Fig. 4.** Stratigraphic records of mantle potential temperature plotted as height relative to the base of the Upper Basalt Formation (UBF). A – olivine-spinel thermometry, corrected for crystallisation, latent heat and adiabatic heat loss. B – Monte Carlo PRIMELT3 (MC-PRIMELT3) temperatures, corrected for clinopyroxene fractionation. For each sample the temperature is plotted with  $1\sigma$  error bars. For LBF and UBF, the mean,  $\pm 1\sigma$  bounds, and range of the sample temperatures is shown by vertical lines and coloured boxes indicating greater variability in mantle temperature during emplacement of the earlier LBF magmas. Horizons marked by thick (>2.5 m) weathering zones are shown as red dotted lines.

elements (Supplementary Figs. S10, S13; [Hole and Natland, 2020](#)). Major elements show correlations with calculated  $T_p$  consistent with their expected behaviour during mantle melting, lending further support to the inferred variation in mantle temperature (Supplementary Text S4.4).

#### 5.1.1. Time-lag in the erupted record of mantle temperatures

Both olivine-spinel and MC-PRIMELT3 temperature records show a distinct interval of markedly lower temperatures in the LBF, 200–250 m below the base of the UBF. However, there is a 20 m stratigraphic offset with the temperature minimum appearing higher in the olivine-spinel dataset (Fig. 4). We interpret this as the result of disequilibrium between olivine phenocrysts and their carrier melt. Erupted melts commonly carry a xenocrystic cargo, derived from remobilisation of residual crustal mushes which form as a result of fractional crystallisation before past eruptions (e.g., [Thomson and MacLennan, 2013](#)). The direction of the offset, with the olivine-spinel temperature anomaly lagging the temperatures based on liquid compositions, is consistent with these olivines being xenocrystic and recording a slightly earlier  $T_p$  than their carrier melt. The presence of xenocrysts would not impact the results of MC-PRIMELT3 modelling since this was performed on calculated olivine-free compositions.

To test the validity of this interpretation, we assess Fe-Mg equilibrium between the cores of olivine macrocrysts and their host liquid, assuming equilibrium  $k_D^{ol/L}$  Fe/Mg of 0.30–0.33 ([Putirka, 2005](#)). Phenocrystic olivine which grew directly from the carrier melt during crustal magma storage and ascent must be in equilibrium with either: 1)

the whole-rock composition of its host rock, 2) the composition of the crystal free liquid (i.e. excluding olivine; calculated for input into MC-PRIMELT3 modelling), or 3) a composition between (1) and (2). Olivines more primitive than any of these could have crystallised from earlier more primitive melts, parental to the erupted lava, whereas olivines which are more evolved than any equilibrium composition are likely xenocrystic and accumulated from pre-existing mush during magma ascent (country-rock derived antecrysts are absent as the ALG intruded through an olivine-free continental basement; [Mitchell, 2004](#)).

Most of our olivine cores are in equilibrium with the whole-rock or crystal-free liquid composition of their host lava or bracketed by the two (Fig. 5). However, in many samples, some or all of the olivines are far from equilibrium with either whole-rock and calculated liquid compositions, indicating a prevalence of xenocrystic material. Samples from the critical interval where the two temperature records are offset (ABB019-ABB023) show abundant evidence for xenocrystic olivine (3–100 % of olivines analysed; Fig. S15). Furthermore, apparent chemical equilibrium between olivine and melt could be coincidental and does not preclude that olivine too being xenocrystic. The presence of coarse grained olivine + plagioclase glomerocrysts in some samples (excluded from PRIMELT3 modelling due to their potentially having equilibrated with plagioclase; Fig. S2) further attests to ascending melts incorporating crustal cumulates, with similar examples well-documented in magmatic systems (e.g., [Holness et al., 2019](#); [Thomson and MacLennan, 2013](#)). This supports our inference that there is not a one-to-one correspondence between the whole-rock and mineral records of temperature: xenocrystic olivines may give temperatures for magmas



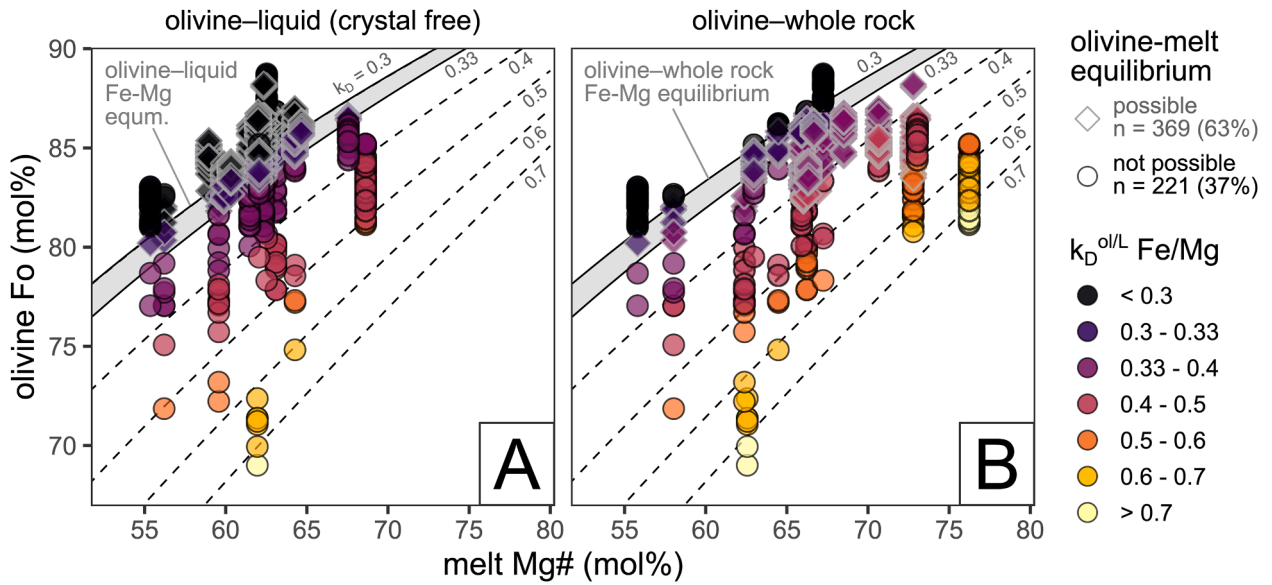


**Fig. 5.** Graphs of melt Mg# versus Fo content showing olivine-melt equilibrium/disequilibrium for olivine phenocryst/macrocryst cores. A – melt composition calculated as olivine free (Supplementary Table S3). B – melt equal to whole rock lava composition. On both plots, contours of  $k_D^{\text{ol/L}} \text{Fe/Mg}$  are shown. Equilibrium  $k_D$  is assumed to be 0.30–0.33. Olivines which may be in equilibrium with either the liquid or whole rock composition are plotted with grey borders and those which are not in equilibrium with black borders. Olivine more primitive than equilibrium compositions ( $k_D < 0.3$ ) may be in equilibrium with more primitive melts parental to their host lava. Olivines too evolved to be in equilibrium ( $k_D \gg 0.33$ ) are likely to be xenocrystic. Histograms showing the distribution of  $k_D$  and proportions of olivine of each equilibrium status separately for every sample are available as Supplementary Figure S15.

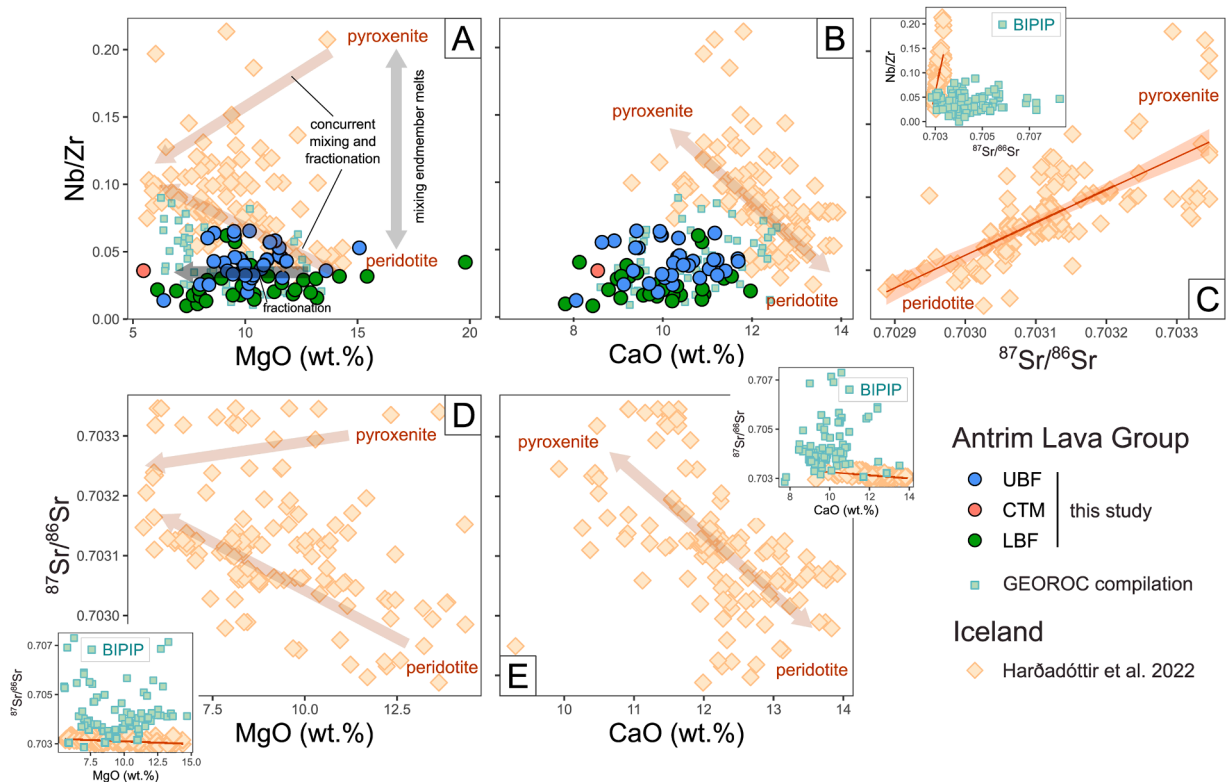


**Fig. 6.** Contrasting evidence for pyroxenite melting in Iceland and Antrim. A-B: Nb/Zr versus major elements (MgO, CaO). Icelandic basalts with MgO between 6 and 14 % and  $^{87}\text{Sr}/^{86}\text{Sr} < 0.70335$  from the filtered compilation of Harðadóttir et al. (2022) are plotted in orange and show mixing between pyroxenite and peridotite derived endmembers (Shorttle et al., 2014). ALG data from this study and the literature are plotted for comparison and do not show evidence for a pyroxenite-derived endmember. C:  $^{87}\text{Sr}/^{86}\text{Sr}$  versus Nb/Zr for Icelandic basalts showing strong correlation between trace element and isotopic tracers of pyroxenite melting. D-E:  $^{87}\text{Sr}/^{86}\text{Sr}$  versus major elements (MgO, CaO) for Icelandic basalts showing similar systematics as A-B, linking isotopic enrichment to lithological heterogeneity. BIPIP basalts (6–14 % MgO) are plotted as insets to panels C-E showing significantly elevated  $^{87}\text{Sr}/^{86}\text{Sr}$ , indicating interaction with continental basement, but no strong correlations between  $^{87}\text{Sr}/^{86}\text{Sr}$  and either Nb/Zr ratios or major elements, suggesting these remain unperturbed. ALG and BIPIP literature data taken from GEOROC (DIGIS Team, 2023). An extended version of this figure including  $\text{FeO}_T$  data is available as Supplementary Figure S10.

which stalled in the crust; vice versa, aphyric lavas may be erupted earlier than their crystal cargo resulting in a temporal offset between MC-PRIMELT3 and olivine-spinel temperatures.

## 5.2. Temporal record of a pulsing plume?

Stratigraphic variation in melting  $T_p$  through the ALG sequence could derive from: 1. heterogeneity in the mantle source, 2. convective instabilities induced by subcontinental lithospheric mantle (SCLM) extension, 3. lateral transport of magmas from cooler and hotter mantle regions, or 4. pulses of hotter and cooler material within a rising plume. Determining which of these mechanisms is plausible places direct constraints on competing models for LIP formation; non-plume “warm” insulated mantle models (e.g. Hole and Natland, 2020) necessitate a steady-state or cooling mantle and, without the additional mechanism of mantle heterogeneity, convective instabilities, or lateral migration of magma (1–3 above) are inconsistent with the stratigraphic  $T_p$  fluctuations observed in our data. We address each of these mechanisms in turn below and show that the first three are unlikely to explain the data and that, instead, our results are consistent with a pulsing plume model.

Variation in the proportion of fusible pyroxenite and refractory harzburgite in the mantle source alters its thermal structure and will lead, respectively, to under- or over-estimation of  $T_p$  from olivine-spinel  $T_{\text{cryst}}$  if assuming a lherzolitic source (Matthews et al., 2016). Elevated Nb/Zr and Zn/Fe ratios in basalts and Ni contents in their olivine phenocrysts have all been used to fingerprint the contributions of pyroxenite during mantle melting (Le Roux et al., 2010; Shorttle et al., 2014; Sobolev et al., 2005). Applied to the ALG magmas, these proxies provide no positive evidence for significant involvement of pyroxenite in their petrogenesis; ALG Nb/Zr ratios are low and do not show correlations with major elements which are characteristic of hybrid peridotite/pyroxenite melts in Iceland (Fig. 6; Shorttle et al., 2014; Shorttle and MacLennan, 2011). Likewise, Zn/Fe ratios and olivine Ni contents are in line with what would be expected of peridotite-derived melts (Fig. 7, Supplementary Figs. S6, S11). While variation in the proportion of mantle harzburgite is theoretically capable of producing nearly the full  $T_p$  variation seen in our dataset (Matthews et al., 2016), such variation would be accompanied by drastic variation in melt productivity. We would therefore expect magmas from refractory harzburgite-rich mantle

with high apparent  $T_p$  to be less abundant than those produced from more fertile mantle with lower apparent  $T_p$ . This is inconsistent with the ALG succession which shows the opposite trend. Consequently, we calculate and interpret  $T_p$  assuming a homogeneous lherzolitic source (see Supplementary Text S4.2.3 for further justification), while acknowledging that we are unable to entirely exclude that some part of the apparent  $T_p$  variation may be due to minor variation in melting lithology which has been masked by subsequent mixing of endmember melts. In such a case our results would suggest a plume that was both thermally and chemically pulsed.

Incipient rifting or plume erosion can create topography at the lithosphere-aesthenosphere boundary, leading to convective foundering and melting of dense metasomatic pyroxene-rich hybrids in the lower-most lithosphere (Brune et al., 2023; Furman et al., 2016). Modelling indicates that such processes can generate small-scale convection cells which juxtapose hot and cold mantle domains on scales of <100 km (Gernon et al., 2023). However, notwithstanding, the lack of geochemical evidence for melting of pyroxenite-rich lithospheric material, rifting did not commence between Greenland and Europe until ~56 Ma (Saunders et al., 1997), precluding this mechanism for generating  $T_p$  variations in the ALG.

Lateral transport of magmas sampling different points across a temperature gradient in the mantle source could generate apparent temporal variation in  $T_p$  recorded by the erupted lavas. Broad temperature gradients have been invoked to explain the spread of temperatures recorded in a variety of ocean islands and LIPs (Herzberg and Gazel, 2009; Hole and Millett, 2016) and lateral magma transport has been offered as an explanation for alkaline-tholeiitic transitions within the BIIP (e.g., Hole et al., 2015; Kent and Fitton, 2000; White, 1992). Mantle thermometry from contemporaneous Western and Eastern Greenland lavas indicate a lateral temperature gradient of ~0.1 °C/km across the NAIP (Hole and Millett, 2016). Applied to our data, this would require >1000 km of lateral transport to explain the maximum temperature variation in the LBF. While such laterally-extensive dyke swarms have been identified (e.g., Ernst and Baragar, 1992), they are rare and it is difficult to envisage how distinct magma compositions, recording very different mantle temperatures, could survive such extensive migration without mixing/homogenisation or freezing in the crust. Furthermore, this mechanism is unable to explain the observed

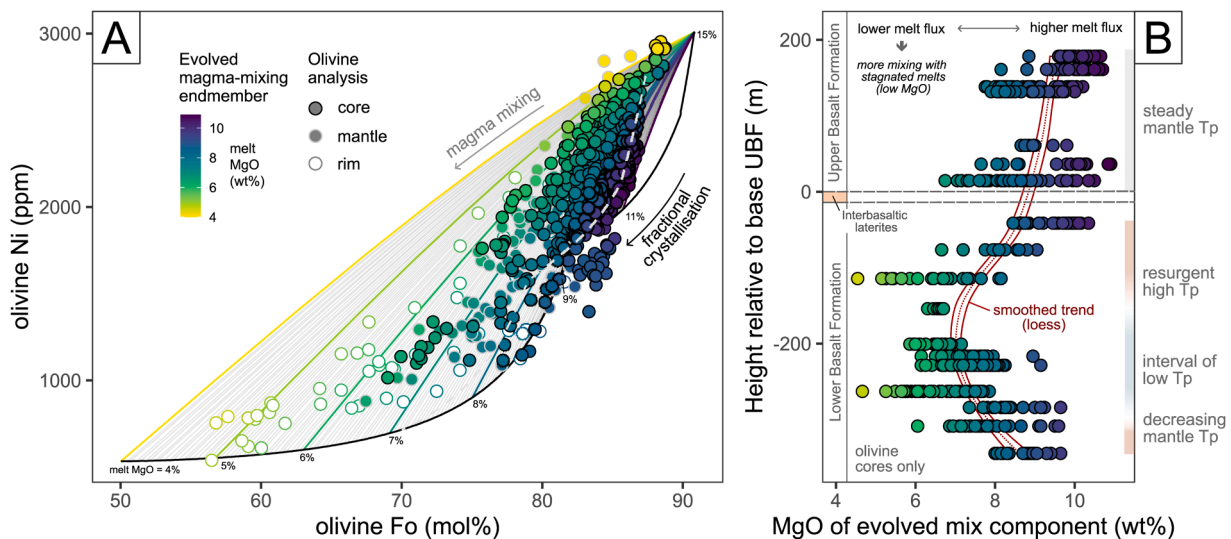


**Fig. 7.** Olivine Ni contents as a proxy for crustal processes. A – olivine Ni versus Fo contents. A crystal line of descent (black) line has been calculated from a primary magma composition as well as the composition of olivine along mixing curves between the primary magma and more evolved magmas derived from it (coloured lines). Olivine data points are colour coded by the MgO content of the evolved mixing endmember required to explain their Ni contents. B – MgO of the evolved mixing component plotted against stratigraphic height relative to the base of the UBF. Olivines compositions record systematic variation in the degree of mixing with evolved magmas with the lowest MgO endmember corresponding to the interval of low mantle temperature. For individual plots of olivine composition by sample see Supplementary Figure S6.

stratigraphic transition from variable to uniform  $T_p$  (i.e., between the LBF and UBF). Hence, we do not consider it to be a viable mechanism for generating the observed ALG  $T_p$  variations.

Instead, we infer that temporal  $T_p$  variations through the ALG arise from thermal pulsing in a mantle plume. Pulsatory or oscillatory dynamics have been demonstrated from a range of studies in Iceland and other ocean islands over timescales ranging from <1 to a few million years (Liu et al., 2023; Parnell-Turner et al., 2014; Spice et al., 2016; Taylor et al., 2020). Although the exact chronostratigraphy of the LBF sequence is unknown, U-Pb geochronology constrains its eruptive period to ~0.5 Ma (Cooper et al., 2020), suggesting that the frequency of temperature variation recorded in the LBF lavas is on the order of <10<sup>5</sup> yrs, and appears to represent the shortest timescales of terrestrial plume pulsing identified to date. Thermal pulses recorded in the ALG have a higher amplitude and order of magnitude shorter periodicity than those of the modern Icelandic plume, inferred from V-shaped ridges (~25 °C; 3–6 Myr; Parnell-Turner et al., 2014). However, it should be noted that crustal thickness in V-shaped ridges is inherently insensitive to variation on the timescale of individual eruptions and instead records long-term average conditions during their assembly; some of the apparent differences in timescale may therefore be down to differing temporal resolutions of the two records.

Plume pulsing provides a viable explanation for the change from variable to steady temperatures between the LBF and UBF, as thermochemical plumes are inherently unstable phenomena and undergo secular changes in state and behaviour. This is recorded empirically by a marked transition in the periodicity and amplitude of Icelandic plume oscillations at ~35 Ma, manifest by the onset of V-shaped ridge formation and a transition to long-term warming (Parnell-Turner et al., 2014; Spice et al., 2016). Periodic and oscillatory behaviours are furthermore predicted by numerical and experimental plume models, arising from boundary condition perturbations, at the core-mantle interface (Olson et al., 1987; Scott et al., 1986). Hence, a punctuated shift from variable to uniform  $T_p$  in the ALG is entirely consistent with our understanding of long-term plume behaviour and dynamics.

### 5.3. Crustal response to fluctuating temperatures

The occurrence of rapid variations in mantle potential temperatures provides an opportunity to investigate the intrinsic link between mantle, crustal and volcanic processes, examining how eruptive and sub-volcanic systems are affected by forcing from the Earth's interior. Olivine phenocrysts preserve an archive of mantle and crustal processes, with their Ni contents varying as a function of mantle melting components (Sobolev et al., 2005) and as a result of crustal magma mixing (Gleeson and Gibson, 2019; Herzberg and Asimow, 2015; Hole, 2018). In our samples olivine Ni concentrations are systematically higher in many LBF samples than the UBF for a given Fo content (Fig. 7), but ubiquitously lower than those anticipated for melting of a pyroxenitic source (<4700 ppm; Sobolev et al., 2005). This is consistent with previous studies in the NAIP and has been taken as evidence against a pyroxenite melting component (Herzberg et al., 2016; Hole, 2018); consequently, variable Ni concentrations in our olivine crystals more likely represent the effect of mixing between mafic and evolved melts (e.g., Gleeson and Gibson, 2019). To verify this, we model the effects of fractional crystallisation and mixing on olivine crystal lines of descent (CLDs; Supplementary Text S4.1).

Results of our olivine CLD models indicate that olivine Ni contents indeed reflect magma mixing. Elevated Ni contents can result from mixing of primary magmas with more evolved (lower MgO) melts, and the Ni content of olivine (at a given Fo content) is inversely proportional to the MgO content of the evolved endmember (Fig. 7a). Elevated Ni at a given Fo content could also arise from mixing of peridotite- and pyroxenite-derived melts. However, the trends defined by individual sample's olivine compositions are close to calculated mixing curve between two peridotite-derived melts and always at a lower angle than

predicted for pyroxenite derived CLDs (Supplementary Figure S6; Shorttle and MacLennan, 2011). Additionally, many ALG olivines plot to higher Ni and lower Fo than a pure KG2 pyroxenite-derived CLD, indicating that mixing with low MgO melts must be the dominant process controlling their Ni contents. Hence, the data strongly support mixing between evolved and primitive melts during the interval of low mantle  $T_p$ , and do not provide any strong support for the involvement of pyroxenite-derived magmas.

The extent of mixing required to produce the observed olivine compositions varies widely (0–90 %) and apparently randomly in all our Antrim samples, but the Ni content of the olivine – and therefore the MgO of the more-evolved mixing component – varies systematically through the stratigraphy (Fig. 7b). In the LBF, olivine Ni contents record variable mixing between near-primary magmas (MgO > 14 %) and both mafic (MgO < 10 wt%) and substantially evolved melts (MgO ~4 wt%), whereas the evolved mixing component in the UBF is restricted to more mafic compositions only (~7–11 wt%). Notably, the most evolved (lowest MgO) mixing component occurs in the middle part of the LBF, at the same stratigraphic level as our calculated low mantle  $T_p$  results (Fig. 7b). This suggests that magmatic flux was not constant during emplacement of the ALG, as this would produce more stable mixing endmember compositions and olivine Ni contents. Rather, mixing of near-primary magmas with more evolved melts in the LBF implies stagnation and intervals of low magmatic flux into the crust. By contrast, in the UBF the evolved mixing component is consistently more mafic, implying a steadier mantle melt flux (e.g., Tapu et al., 2023). The correlation between these results and our mantle temperature record suggests that the extent to which crustal melts stagnate and evolve is controlled from below and driven by a decrease in primary melt productivity in response to fluctuations in mantle  $T_p$ .

Insight into the tempo of surface volcanism during emplacement of the ALG can be derived from the degree of weathering of individual lava flows. Antrim lava flows are commonly capped by a reddened zone of incipient lateritisation, resulting from sub-aerial alteration (Hill et al., 2000). These form slowly from the top down and their thickness provides a proxy for the repose period between successive eruptions (Beresford-Browne et al., 2024; Zehetner et al., 2020). The abundance of thick alteration zones (>2.5 m) is markedly higher in the LBF than the UBF within our composite stratigraphy: the LBF contains six flows which are capped by 2.5–5 m thick weathering horizons whereas the UBF contains just one. Additionally, the top of the LBF is capped by a thick laterite layer which marks the interbasaltic hiatus between LBF and UBF (Fig. 8).

Although weathering rates are impacted by climatic conditions, benthic isotope records indicate only a moderate increase in global temperatures during ALG emplacement (~61.5–58.5 Ma; Westerhold et al., 2020); thus, climatic effects would favour greater alteration of the UBF than the LBF, in contrast with the observed stratigraphy. Instead, we ascribe variations in sub-aerial alteration extent to real temporal variations in eruption frequency, whereby LBF eruptions were more sporadic with periodic extended hiatuses in activity and UBF eruptions were emplaced at a steadier rate with consistently short repose times (Fig. 8b). Accompanying this irregular rhythm of volcanism, mantle temperature and melt flux were also highly variable during emplacement of the LBF. Although there is not a direct one-to-one correlation between the thickness of weathering horizons and mantle  $T_p$ , all but one thick weathering horizon is preceded by a drop in temperature. Furthermore, it should be noted that the response of a complex volcano-magmatic system to perturbation is very unlikely to be linear especially at a single location (e.g., Sparks, 2003).

We suggest that variability in mantle  $T_p$  and crustal melt flux not only impacted the extent to which sub-volcanic melts evolved, but potentially also the tempo of volcanism at Earth's surface. Hence, our stratigraphically controlled dataset demonstrates a first-order link between variations (or lack thereof) in mantle  $T_p$  and subsequent crustal and volcanic processes during magma ascent and eruption. This further

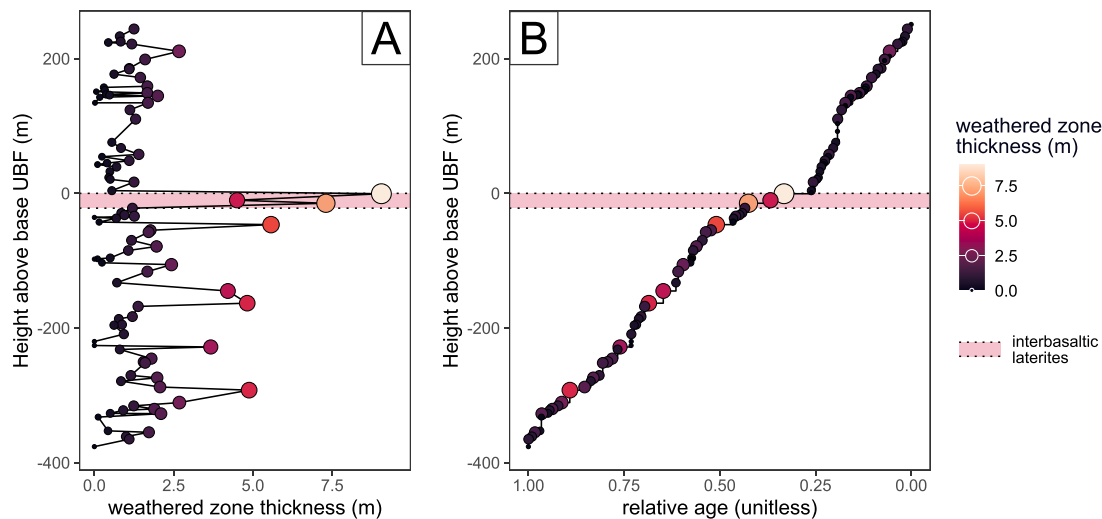


**Fig. 8.** Variation in the tempo of volcanism. A – the thickness of the weathered layer of each lava flow plotted against stratigraphic height relative to the base of the UBF. Thick weathering layers are more abundant in the LBF. B – relative age of lavas plotted against stratigraphic height. Relative age was calculated assuming weathered layer thickness is linearly proportional to repose period. The top and bottom of the interbasaltic laterites are indicated on both panels by a dotted line and the pink highlighted region.

raises the possibility that a major and long-lived decrease in mantle temperature was also responsible for the prolonged volcanic hiatus and lateritic development between UBF and LBF.

## 6. Conclusions

By applying two independent methods of thermometry within a robust stratigraphic framework we are able, for the first time, to establish high resolution temporal variations in mantle potential temperature ( $T_p$ ) through the early stages of a major LIP at the scale of individual lava flows. The results indicate marked variation in  $T_p$ , with olivine-spinel thermometry yielding a range of 1403–1521 °C and Monte Carlo PRIMELT3 modelling 1374–1472 °C. Temperature variation is significantly higher in the LBF than the UBF, with an interval of distinctly low  $T_p$  (~200 m depth) in the LBF sequence recorded by both thermometers. This temporal variation in mantle potential temperatures is very difficult to explain via non-plume models for LIP formation but is readily explained by pulsatory behaviour in the proto-Icelandic plume, with periodic hotter and cooler material originating from perturbations at the core mantle boundary.

The nickel content of olivine can be used as a proxy for melt flux into the crustal magmatic system and implies systematically lower melt flux in the LBF following the interval of low temperatures. Similarly, the abundance of thick weathering horizons is also much higher in the LBF than the UBF, indicating more variable repose period between eruptions. These observations together link the mantle, crustal and volcanic systems during LIP formation, indicating that variations in mantle  $T_p$  can significantly influence magmatic dynamics and perhaps the tempo of volcanism. This in turn suggests that the particular behaviour of a mantle plume (i.e., pulsing versus steady), and changes therein, may be an important driving force, mediating the tempo and evolution of volcanism in large igneous provinces and potentially at modern ocean islands.

## CRediT authorship contribution statement

**Elliot J. Carter:** Writing – review & editing, Writing – original draft, Visualization, Validation, Software, Project administration, Methodology, Investigation, Funding acquisition, Formal analysis, Data curation, Conceptualization. **Michael J. Stock:** Writing – review & editing, Supervision, Resources, Project administration, Funding acquisition, Conceptualization. **Adam Beresford-Browne:** Writing – review &

editing, Resources, Methodology, Data curation. **Mark R. Cooper:** Writing – review & editing, Resources. **Robert Raine:** Writing – review & editing, Resources. **Alexia Fereyrolles:** Investigation, Data curation.

## Declaration of competing interest

The authors declare that they have no known competing financial interests or personal relationships that could have appeared to influence the work reported in this paper.

## Data availability

All supporting data - including all geochemical data and outputs from models discussed in the text - have been made available as Supplementary Tables S1-S10 which accompany this manuscript.

## Acknowledgements

This work was supported by an Irish Research Council Fellowship awarded to EC (GOIPD/2020/917) and a Science Foundation Ireland and Geological Survey Ireland co-funded Frontiers for the Future Programme grant awarded to MS (20/FFP-P/8895). The authors would like to thank Oliver Higgins for helpful comments and discussion regarding Monte Carlo methods and thermometry. Clara Amaral and Sarah Carty are also thanked for their technical assistance with XRF preparation and, likewise, Iris Buisman for assistance with EPMA and Francis Hendron for assistance with sample preparation. Vincent Salters and an anonymous reviewer are thanked for their insightful comments which helped strengthen this manuscript, and Chiara Maria Petrone is thanked for her editorial handling. We are grateful to Geological Survey Ireland for permitting and funding access to the Earth Surface Research Laboratory for XRF analysis, and to the Geological Survey of Northern Ireland for allowing access to core samples without which this work wouldn't have been possible.

## Supplementary materials

Supplementary material associated with this article can be found, in the online version, at [doi:10.1016/j.epsl.2024.118903](https://doi.org/10.1016/j.epsl.2024.118903).



## References

- Anderson, D.L., Zhang, Y.-S., Tanimoto, T., 1992. Plume heads, continental lithosphere, flood basalts and tomography. *Geol. Soc. Lond. Spec. Publ.* 68, 99–124. <https://doi.org/10.1144/GSL.SP.1992.068.01.07>.
- Anderson, H., Walsh, J., Cooper, M., 2016. Faults, intrusions and flood basalts: the Cenozoic structure of the north of Ireland. In: Young, M.E. (Ed.), *Unearthed: Impacts of the Tellus Surveys of the North of Ireland*. Royal Irish Academy, Dublin. <https://doi.org/10.3318/978-1-908996-88-6.ch14>.
- Bailey, E.B., Clough, C.T., Wright, W.B., Richey, J.E., Wilson, G.V., 1924. Tertiary and post-tertiary geology of Mull, Loch Aline, and Oban: a description of parts of sheets 43, 44, 51, and 52 of the geological map. HM Stationery Office.
- Barrat, J.A., Nesbitt, R.W., 1996. Geochemistry of the tertiary volcanism of northern Ireland. *Chem. Geol.* 129, 15–38.
- Beresford-Browne, A., Jolley, D., Millett, J., Stevenson, C., Watt, S., Raine, R., Carter, E., 2024. Depositional system and plant ecosystem responses to long-term low tempo volcanism, the Interbasaltic Formation, Antrim Lava Group. *Geol. Soc. Lond. Spec. Publ.* 547 <https://doi.org/10.1144/SP547-2023-75>.
- Black, B.A., Karlstrom, L., Mather, T.A., 2021. The life cycle of large igneous provinces. *Nat. Rev. Earth Environ.* 2, 840–857. <https://doi.org/10.1038/s43017-021-00221-4>.
- Brune, S., Kolawole, F., Olive, J.-A., Stamps, D.S., Buck, W.R., Buiter, S.J.H., Furman, T., Shillington, D.J., 2023. Geodynamics of continental rift initiation and evolution. *Nat. Rev. Earth Environ.* 4, 235–253. <https://doi.org/10.1038/s43017-023-00391-3>.
- Campbell, I.H., 2007. Testing the plume theory. *Chem. Geol.* 241, 153–176. <https://doi.org/10.1016/j.chemgeo.2007.01.024>.
- Chambers, L.M., Fitton, J.G., 2000. Geochemical transitions in the ancestral Iceland plume: evidence from the Isle of Mull Tertiary volcano, Scotland. *J. Geol. Soc.* 157, 261–263. <https://doi.org/10.1144/jgs.157.2.261>.
- Clapham, M.E., Renne, P.R., 2019. Flood basalts and mass extinctions. *Annu. Rev. Earth Planet. Sci.* 47, 275–303. <https://doi.org/10.1146/annurev-earth-053018-060136>.
- Coogan, L.A., Saunders, A.D., Wilson, R.N., 2014. Aluminum-in-olivine thermometry of primitive basalts: evidence of an anomalously hot mantle source for large igneous provinces. *Chem. Geol.* 368, 1–10. <https://doi.org/10.1016/j.chemgeo.2014.01.004>.
- Cooper, M., Tapster, S., Condon, D., 2020. New high resolution U-Pb zircon geochronological constraints for the Northern Ireland sector of the North Atlantic Igneous Province (No. EGU2020-8464). Presented at the EGU2020. Copernicus Meetings. <https://doi.org/10.5194/egusphere-egu2020-8464>.
- Cooper, M.R., 2004. Mantle plumes, ocean spreading and the North Atlantic Igneous Province, Palaeogene extrusive igneous rocks. *The Geology of Northern Ireland-Our Natural Foundation*. Geological Survey of Northern Ireland. Northern Ireland, Belfast.
- Danyushevsky, L.V., Plechov, P., 2011. Petrolog3: integrated software for modeling crystallization processes. *Geochem. Geophys. Geosystems* 12. <https://doi.org/10.1029/2011GC003516>.
- DIGIS Team, 2023. GEOROC Compilation: Continental Flood Basalts, GRO.data, V9. <https://doi.org/10.25625/WSTPOX>.
- Ellam, R.M., Stuart, F.M., 2000. The sub-lithospheric source of North Atlantic basalts: evidence for, and significance of, a common end-member. *J. Petrol.* 41, 919–932. <https://doi.org/10.1093/petrology/41.7.919>.
- Ernst, R.E., Baragar, W.R.A., 1992. Evidence from magnetic fabric for the flow pattern of magma in the Mackenzie giant radiating dyke swarm. *Nature* 356, 511–513. <https://doi.org/10.1038/356511a0>.
- Fitton, J.G., Saunders, A.D., Norry, M.J., Hardarson, B.S., Taylor, R.N., 1997. Thermal and chemical structure of the Iceland plume. *Earth Planet. Sci. Lett.* 153, 197–208. [https://doi.org/10.1016/S0012-821X\(97\)00170-2](https://doi.org/10.1016/S0012-821X(97)00170-2).
- Foulger, G.R., Anderson, D.L., 2005. A cool model for the Iceland hotspot. *J. Volcanol. Geotherm. Res.* 141, 1–22. <https://doi.org/10.1016/j.jvolgeores.2004.10.007>.
- Furman, T., Nelson, W.R., Elkins-Tanton, L.T., 2016. Evolution of the East African rift: drip magmatism, lithospheric thinning and mafic volcanism. *Geochim. Cosmochim. Acta* 185, 418–434. <https://doi.org/10.1016/j.gca.2016.03.024>. Magmas and their sources: A special issue honoring Frederick A. Frey.
- Gernon, T.M., Jones, S.M., Brune, S., Hincks, T.K., Palmer, M.R., Schumacher, J.C., Primiceri, R.M., Field, M., Griffin, W.L., O'Reilly, S.Y., Keir, D., Spencer, C.J., Merdith, A.S., Glerum, A., 2023. Rift-induced disruption of cratonic keels drives kimberlite volcanism. *Nature* 620, 344–350. <https://doi.org/10.1038/s41586-023-06193-3>.
- Gleeson, M.L.M., Gibson, S.A., 2019. Crustal controls on apparent mantle pyroxenite signals in ocean-island basalts. *Geology* 47, 321–324. <https://doi.org/10.1130/G45759.1>.
- Herzberg, C., Asimow, P.D., 2015. PRIMELT3 MEGA.XLSM software for primary magma calculation: peridotite primary magma MgO contents from the liquidus to the solidus. *Geochem. Geophys. Geosystems* 16, 563–578. <https://doi.org/10.1002/2014GC005631>.
- Harðardóttir, S., Matthews, S., Halldórsson, S.A., Jackson, M.G., 2022. Spatial distribution and geochemical characterization of Icelandic mantle end-members: Implications for plume geometry and melting processes. *Chem. Geol.* 604, 120930. <https://doi.org/10.1016/j.chemgeo.2022.120930>.
- Herzberg, C., Asimow, P.D., 2008. Petrology of some oceanic island basalts: PRIMELT2. XLS software for primary magma calculation. *Geochem. Geophys. Geosystems* 9. <https://doi.org/10.1029/2008GC002057>.
- Herzberg, C., Asimow, P.D., Arndt, N., Niu, Y., Leshner, C.M., Fitton, J.G., Cheadle, M.J., Saunders, A.D., 2007. Temperatures in ambient mantle and plumes: constraints from basalts, picrites, and komatiites: Mantle temperatures inferred from volcanoes. *Geochem. Geophys. Geosystems* 8. <https://doi.org/10.1029/2006GC001390> n/a-n/a.
- Herzberg, C., Gazel, E., 2009. Petrological evidence for secular cooling in mantle plumes. *Nature* 458, 619–622. <https://doi.org/10.1038/nature07857>.
- Herzberg, C., Vidito, C., Starkey, N.A., 2016. Nickel–cobalt contents of olivine record origins of mantle peridotite and related rocks. *Am. Mineral.* 101, 1952–1966. <https://doi.org/10.2138/am-2016-5538>.
- Hill, I.G., Worden, R.H., Meighan, I.G., 2000. Geochemical evolution of a palaeolaterite: the Interbasaltic formation, Northern Ireland. *Chem. Geol.* 166, 65–84. [https://doi.org/10.1016/S0009-2541\(99\)00179-5](https://doi.org/10.1016/S0009-2541(99)00179-5).
- Hirschmann, M.M., Ghiorso, M.S., Davis, F.A., Gordon, S.M., Mukherjee, S., Grove, T.L., Krawczynski, M., Medard, E., Till, C.B., 2008. Library of Experimental Phase Relations (LEPR): a database and web portal for experimental magmatic phase equilibria data. *Geochem. Geophys. Geosystems* 9. <https://doi.org/10.1029/2007GC001894>.
- Hole, M.J., 2018. Mineralogical and geochemical evidence for polybaric fractional crystallization of continental flood basalts and implications for identification of peridotite and pyroxenite source lithologies. *Earth-Sci. Rev.* 176, 51–67. <https://doi.org/10.1016/j.earscirev.2017.09.014>.
- Hole, M.J., Millett, J.M., 2016. Controls of mantle potential temperature and lithospheric thickness on magmatism in the North Atlantic igneous province. *J. Petrol.* 57, 1–20. <https://doi.org/10.1093/petrology/egw014>.
- Hole, M.J., Millett, J.M., Rogers, N.W., Jolley, D.W., 2015. Rifting and mafic magmatism in the hebridean basins. *J. Geol. Soc.* 172, 218–236. <https://doi.org/10.1144/jgs2014-100>.
- Hole, M.J., Natland, J.H., 2020. Magmatism in the North Atlantic Igneous Province: mantle temperatures, rifting and geodynamics. *Earth-Sci. Rev.* 206, 102794. <https://doi.org/10.1016/j.earscirev.2019.02.011>.
- Holness, M.B., Stock, M.J., Geist, D., 2019. Magma chambers versus mush zones: constraining the architecture of sub-volcanic plumbing systems from microstructural analysis of crystalline enclaves. *Philos. Trans. R. Soc. Math. Phys. Eng. Sci.* 377, 20180006. <https://doi.org/10.1098/rsta.2018.0006>.
- Katsura, T., 2022. A Revised Adiabatic Temperature Profile for the Mantle. *J. Geophys. Res. Solid Earth* 127, e2021JB023562. <https://doi.org/10.1029/2021JB023562>.
- Kent, R.W., Fitton, J.G., 2000. Mantle sources and melting dynamics in the British Palaeogene igneous province. *J. Petrol.* 41, 1023–1040. <https://doi.org/10.1093/petrology/41.7.1023>.
- Kimura, J.-I., Ariskin, A.A., 2014. Calculation of water-bearing primary basalt and estimation of source mantle conditions beneath arcs: PRIMACALC2 model for WINDOWS. *Geochem. Geophys. Geosystems* 15, 1494–1514. <https://doi.org/10.1002/2014GC005329>.
- King, S.D., 2007. Hotspots and edge-driven convection. *Geology* 35, 223–226. <https://doi.org/10.1130/G23291A.1>.
- Le Roux, V., Lee, C.-T.A., Turner, S.J., 2010. Zn/Fe systematics in mafic and ultramafic systems: implications for detecting major element heterogeneities in the Earth's mantle. *Geochim. Cosmochim. Acta* 74, 2779–2796. <https://doi.org/10.1016/j.gca.2010.02.004>.
- Lee, C.T.A., Luffi, P., Plank, T., Dalton, H., Leeman, W.P., 2009. Constraints on the depths and temperatures of basaltic magma generation on Earth and other terrestrial planets using new thermobarometers for mafic magmas. *Earth Planet. Sci. Lett.* 279, 20–33. <https://doi.org/10.1016/j.epsl.2008.12.020>.
- Liu, H., Leng, W., Wang, W., Zheng, Y., 2023. Deciphering the deep Earth heterogeneities from the temperature fluctuation of mantle plumes. *Earth Planet. Sci. Lett.* 618, 118275. <https://doi.org/10.1016/j.epsl.2023.118275>.
- Lyle, P., 1985. The petrogenesis of the Tertiary basaltic and intermediate lavas of northeast Ireland. *Scott. J. Geol.* 21, 71–84. <https://doi.org/10.1144/sjg21010071>.
- Lyle, P., Patton, D.J.S., 1989. The petrography and geochemistry of the upper basalt formation of the antrim lava group in northeast Ireland. *Ir. J. Earth Sci.* 10, 33–41.
- Lyle, P., Preston, J., 1993. Geochemistry and volcanology of the tertiary basalts of the giant's causeway area, northern Ireland. *J. Geol. Soc.* 150, 109–120. <https://doi.org/10.1144/gsjgs.150.1.0109>.
- MacLennan, J., McKenzie, D., Gronvold, K., 2001. Plume-driven upwelling under central Iceland. *Earth Planet. Sci. Lett.* 194, 67–82. [https://doi.org/10.1016/S0012-821X\(01\)00553-2](https://doi.org/10.1016/S0012-821X(01)00553-2).
- Matthews, S., Shorttle, O., MacLennan, J., 2016. The temperature of the Icelandic mantle from olivine-spinel aluminum exchange thermometry. *Geochem. Geophys. Geosystems* 17, 4725–4752. <https://doi.org/10.1002/2016GC006497>.
- Matthews, S., Wong, K., Shorttle, O., Edmonds, M., MacLennan, J., 2021. Do olivine crystallization temperatures faithfully record mantle temperature variability? *Geochem. Geophys. Geosystems* 22, 1–32. <https://doi.org/10.1029/2020GC009157>.
- Meyer, R., Van Wijk, J., Gernigon, L., 2007. The North Atlantic Igneous Province: a review of models for its formation. *Spec. Pap. Geol. Soc. Am.* 430, 525–552. [https://doi.org/10.1130/2007.2430\(26](https://doi.org/10.1130/2007.2430(26).
- Mitchell, W., 2004. *The geology of Northern Ireland: our natural foundation*. Geological Survey of Northern Ireland.
- Morgan, W.J., 1971. Convection plumes in the lower mantle. *Nature* 230, 42–43. <https://doi.org/10.1038/230042a0>.
- Olson, P., Schubert, G., Anderson, C., 1987. Plume formation in the D<sup>+</sup>-layer and the roughness of the core–mantle boundary. *Nature* 327, 409–413. <https://doi.org/10.1038/327409a0>.
- Parnell-Turner, R., White, N., Henstock, T., Murton, B., MacLennan, J., Jones, S.M., 2014. A continuous 55-million-year record of transient mantle plume activity beneath Iceland. *Nat. Geosci.* 7, 914–919. <https://doi.org/10.1038/ngeo2281>.
- Patterson, E.M., Swaine, D.J., 1955. The middle lavas of the antrim plateau. *Geochem. Cosmochim. Acta* 8 (173), 181 to.
- Putirka, K.D., 2005. Mantle potential temperatures at Hawaii, Iceland, and the mid-ocean ridge system, as inferred from olivine phenocrysts: evidence for thermally driven

- mantle plumes. *Geochem. Geophys. Geosystems* 6. <https://doi.org/10.1029/2005GC000915> n/a-n/a.
- Saunders, A.D., Fitton, J.G., Kerr, A.C., Norry, M.J., Kent, R.W., 1997. The north atlantic igneous province. Large Igneous Provinces: Continental, Oceanic, and Planetary Flood Volcanism. *Geophysical Monograph* 100, 45–93. <https://doi.org/10.1029/GM100p0045>.
- Scott, D.R., Stevenson, D.J., Whitehead, J.A., 1986. Observations of solitary waves in a viscously deformable pipe. *Nature* 319, 759–761. <https://doi.org/10.1038/319759a0>.
- Shorttle, O., MacLennan, J., 2011. Compositional trends of Icelandic basalts: implications for short-length scale lithological heterogeneity in mantle plumes. *Geochem. Geophys. Geosystems* 12. <https://doi.org/10.1029/2011GC003748>.
- Shorttle, O., MacLennan, J., Lambart, S., 2014. Quantifying lithological variability in the mantle. *Earth Planet. Sci. Lett.* 395, 24–40. <https://doi.org/10.1016/j.epsl.2014.03.040>.
- Sobolev, A.V., Hofmann, A.W., Sobolev, S.V., Nikogosian, I.K., 2005. An olivine-free mantle source of Hawaiian shield basalts. *Nature* 434, 590–597. <https://doi.org/10.1038/nature03411>.
- Sparks, R.S.J., 2003. Forecasting volcanic eruptions. *Earth Planet. Sci. Lett.* 210, 1–15. [https://doi.org/10.1016/S0012-821X\(03\)00124-9](https://doi.org/10.1016/S0012-821X(03)00124-9).
- Spice, H.E., Fitton, J.G., Kirstein, L.A., 2016. Temperature fluctuation of the Iceland mantle plume through time. *Geochem. Geophys. Geosystems* 17, 243–254. <https://doi.org/10.1002/2015GC006059>.
- Stuart, F.M., Lass-Evans, S., Fitton, J.G., Ellam, R.M., 2003. High  $^3\text{He}/^4\text{He}$  ratios in picritic basalts from Baffin Island and the role of a mixed reservoir in mantle plumes. *Nature* 424, 57–59. <https://doi.org/10.1038/nature01711>.
- Tapu, A.T., Ubide, T., Vasconcelos, P.M., 2023. Increasing complexity in magmatic architecture of volcanoes along a waning hotspot. *Nat. Geosci.* <https://doi.org/10.1038/s41561-023-01156-9>.
- Taylor, R.N., Davila-Harris, P., Branney, M.J., Ruth Farley, E.M., Gernon, T.M., Palmer, M.R., 2020. Dynamics of a chemically pulsing mantle plume. *Earth Planet. Sci. Lett.* 537, 116182 <https://doi.org/10.1016/j.epsl.2020.116182>.
- Thompson, R.N., Gibson, S.A., 2000. Transient high temperatures in mantle plume heads inferred from magnesian olivines in Phanerozoic picrites. *Nature* 407, 502–506. <https://doi.org/10.1038/35035058>.
- Thomson, A., MacLennan, J., 2013. The distribution of olivine compositions in icelandic basalts and picrites. *J. Petrol.* 54, 745–768. <https://doi.org/10.1093/petrology/egs083>.
- Till, C.B., Grove, T.L., Krawczynski, M.J., 2012. A melting model for variably depleted and enriched lherzolite in the plagioclase and spinel stability fields. *J. Geophys. Res. Solid Earth* 117. <https://doi.org/10.1029/2011JB009044>.
- Trela, J., Gazel, E., Sobolev, A.V., Moore, L., Bizimis, M., Jicha, B., Batanova, V.G., 2017. The hottest lavas of the Phanerozoic and the survival of deep Archaean reservoirs. *Nat. Geosci.* 10, 451–456. <https://doi.org/10.1038/ngeo2954>.
- Wallace, J.M., Ellam, R.M., Meighan, I.G., Lyle, P., Rogers, N.W., 1994. Sr isotope data for the Tertiary lavas of Northern Ireland: evidence for open system petrogenesis. *J. Geol. Soc.* 151, 869–877. <https://doi.org/10.1144/gsjgs.151.5.0869>.
- Weis, D., Harpp, K.S., Harrison, L.N., Boyet, M., Chauvel, C., Farnetani, C.G., Finlayson, V.A., Lee, K.K.M., Parai, R., Shahar, A., Williamson, N.M.B., 2023. Earth's mantle composition revealed by mantle plumes. *Nat. Rev. Earth Environ.* 1–22. <https://doi.org/10.1038/s43017-023-00467-0>.
- Westerhold, T., Marwan, N., Drury, A.J., Liebrand, D., Agnini, C., Anagnostou, E., Barnett, J.S.K., Bohaty, S.M., De Vleeschouwer, D., Florindo, F., Frederichs, T., Hodell, D.A., Holbourn, A.E., Kroon, D., Lauretano, V., Littler, K., Lourens, L.J., Lyle, M., Pälike, H., Röhl, U., Tian, J., Wilkens, R.H., Wilson, P.A., Zachos, J.C., 2020. An astronomically dated record of Earth's climate and its predictability over the last 66 million years. *Science* 369, 1383–1387. <https://doi.org/10.1126/science.aba6853>.
- White, R.S., 1992. Crustal structure and magmatism of North Atlantic continental margins. *J. Geol. Soc.* 149, 841–854. <https://doi.org/10.1144/gsjgs.149.5.0841>.
- Zehetner, F., Gerzabek, M.H., Shellnutt, J.G., Ottner, F., Lüthgens, C., Miggins, D.P., Chen, P.-H., Candra, I.N., Schmidt, G., Rechberger, M.V., Sprafke, T., 2020. Linking rock age and soil cover across four islands on the Galápagos archipelago. *J. South Am. Earth Sci.* 99, 102500 <https://doi.org/10.1016/j.jsames.2020.102500>.